

RAMAN SPECTROSCOPY AS A PROBE OF SURFACE OXIDES AND HYDRIDES OF NIOBIUM*

J.F. Zasadzinski, B. Albee, C. Cao, S. Bishnoi, IIT Physics/Chemistry, Chicago, IL 60616 USA

D. Ford, Dept. of Chemical/Biological Engineering, NU, Evanston, IL 60208 USA

L. Cooley FNAL, Batavia, IL 60510 USA

T. Proslie, ANL, Argonne, IL 60439

G. Ciovati, JLab, Newport News, VA 23606 USA

Abstract

Raman microscopy/spectroscopy measurements are presented on high purity niobium (Nb) samples and compared with density functional theory (DFT) calculations of vibrational modes of expected surface Nb complexes. The technique is shown to be an effective probe of surface oxides and hydrides of Nb relevant for superconducting radio frequency cavity (SRF) development. A principal result of the work is the observation, in the ordinary Raman backscattering, of Nb hydrides in rough patches (pits) of samples and in cold-worked regions of annealed Nb foils. This indicates that regions of high dislocation density attract hydrogen and form ordered hydride phases of sufficient size to be detected by Raman. Such phases are expected to suppress the local superconductivity and this may explain the connection between hot spots in SRF cavities and the observation of surface pits.

The ordinary Raman backscatter from smooth regions of Nb crystals is relatively featureless but surface enhanced Raman spectroscopy (SERS) has been achieved using deposited Au islands on the Nb. The SERS signal shows a highly reproducible spectrum consisting of dissolved hydrogen in Nb along with broadened peaks from hydride phases indicating hydrogen is present at some level in the near-surface of all Nb samples.

Surface oxides are clearly observed in the Raman spectrum of Nb powders and exhibit changes after a mild baking procedure similar to that used in SRF cavities to mitigate high-field Q-slope problems.

INTRODUCTION

It has been shown recently [1] that localized regions of high dissipation, "hot spots", occurred in a single-cell Nb SRF cavity, fabricated using a buffered chemical polish (BCP), that displayed a medium field Q slope. Furthermore, optical and electron backscattered diffraction (EBSD) imaging showed clearly that such hot spots were correlated with a high area density of etch pits, especially near grain boundaries. Cold spots had more shallow pits of significantly lower density. It is thus of high interest to examine in detail how etch pits might become a source of enhanced local RF dissipation, as chemical etching is integral to the fabrication of cavities.

* Work supported by DOE-HEP through FNAL Laboratory-University Collaboration to Understand Performance Limits of SRF Cavities

The standard spectroscopy tools of EBSD, namely Auger and energy dispersive x-ray, showed little difference between the regions inside and outside the pit. This is not surprising as such spectroscopic tools are cannot measure hydrogen, a gas which diffuses easily in Nb and is a well-known contaminant potentially affecting the cavity Q. [2] Also, these techniques measure an average composition over a relatively large electron probing depth, ~40 nm, and thus would be insensitive to subtle changes in surface oxide composition occurring over ~ 5 nm. This can be significant as it has been shown that < 3 % oxygen vacancies in Nb₂O₅ changes this compound from a nonmagnetic insulator to a conductor with localized magnetic moments. [3] The superconducting gap region probed by tunneling exhibits a smeared density of states consistent with pair breaking due to magnetic scattering. [4] There is thus a good chance that the source of RF dissipation in a pit is tied to the local chemistry, (e.g. oxides, hydrides, dissolved gases) near the surface which might suppress the superconductivity in a variety of ways and cause increased RF impedance and dissipation.

The need for continued development of surface analytical tools for SRF cavities is clear. Here we present Raman microscopy/spectroscopy, a technique which has not previously been used for Nb SRF cavity research. Raman is a simple, fast, non-perturbative optical method which reveals vibrational modes and phonons via inelastic scattering. As will be shown, Raman reveals surface molecular complexes of Nb not easily seen by other techniques. The probing depth (~10-20 nm), is estimated from the skin depth of the 785 nm laser in Nb and is a reasonable fraction of the magnetic penetration depth, ~ 45 nm. Furthermore, Raman has the potential to be an *in-situ* probe of completed SRF cavities by using optical fiber methods.

A comparison of Raman spectra with density functional theory (DFT) calculations of expected molecular complexes allows the identification of hydride and oxide phases. A principal discovery of the present work is the consistent observation of sharp, Raman peaks in regions of Nb which likely contain a high density of dislocations such as etch pits or cold-worked regions. Such peaks are not seen in smooth regions of Nb crystals or recrystallized foils, both of which are expected to have a low concentration of dislocations. These peaks are linked to Nb-H complexes, in particular, ordered hydride phases

suggesting that regions of high dislocation density attract hydrogen with sufficient concentration to form inclusions of stable compounds. This may have relevance to the correlation of hot spots in SRF cavities with the observation of a high density of etch pits.

The technique is extended to surface enhanced Raman spectroscopy (SERS) using an overlayer of Au islands on the Nb surface. The Au islands resonate under the incident laser providing an amplification of the local electric field and enhancement of the Raman scattered light in regions near the Au. The SERS method is more sensitive and it is found that dissolved hydrogen and hydride phases are always present at trace levels and likely adjacent to the oxide layers. However, etch pits have a significantly higher concentration of hydrogen in the sub-surface.

The observation of oxide modes by Raman is most clearly observed in Nb powders. It is found that the standard mild bake (24 hrs at 120 C) used on Nb cavities results in a clear change in the Raman spectrum of the oxide modes suggesting a change in the relative concentrations of Nb₂O₅ and NbO₂.

EXPERIMENT/DFT

All Raman measurements were done using a Renishaw, inVia, Raman microscope with a 785nm laser source, 30s exposure time, 100% laser power [27mW], and a 50X objective which produced a laser spot size $\sim 3\mu\text{m}$ diameter. The small spot size allowed a clear delineation between spectra inside rough regions (typically 10-100 μm in size) with surrounding smooth regions. Several spectra were taken in a region and a spatial average obtained. Corresponding AFM images were obtained in similar regions.

The types of Nb samples studied included high purity powders, foils and single crystals (2mmX2mmX6mm) cut out from a large-grained Nb sheet. We also have preliminary Raman data from actual hot spot samples [1], but these results still need further analysis and will be part of a future publication. High purity foils labeled as unprocessed were as received from Alpha Aesar. Some foils were given a BCP or EP etch similar to that used on cavities. Recrystallized foils are those that were first electropolished and then subjected to a high vacuum (1×10^{-7} torr) anneal up to the Nb melting point. Such foils showed single crystal regions up to a few mm diameter and would be expected to have minimal dislocation density. Such foils were subsequently cold-worked by bending back and forth about 20 times. The Nb powder was 220 mesh which consisted of grains ranging from 40 μm down to 1 μm as measured by SEM. Commercial oxide powders of Nb₂O₅, NbO₂ and NbO were also measured by Raman to compare with DFT calculations and to serve as templates for the identification of surface oxides on the Nb samples.

All calculations were performed with the Vienna Ab initio Simulation Package (VASP)[5,6], using density functional theory (DFT) and a planewave basis set with a

400 eV kinetic energy cutoff. The generalized gradient approximation (GGA) was used with the Perdew, Burke, Ernzerhof (PBE) [7] exchange-correlation functional, and the core electrons were described by the Projector-Augmented-Wave (PAW)[8,9] pseudopotentials.

The geometry was optimized for each crystal structure with a 0.25/Å gamma centered k-point mesh determined from the Monkhorst-Pack scheme [10]. For metallic structures (all except for NbO₂ and Nb₂O₅) the partial occupancies for the wavefunctions were set by the 1st order Methfessel-Paxton method with a smearing width of 0.2 eV, and for the nonmetallic structures the tetrahedron method with Blöchl corrections was used. The α and α' niobium hydride phases were modeled as unit cells of 16 niobium atoms in bcc arrangement with hydrogen atoms randomly inserted into the tetrahedral interstices.

The phonon spectra were calculated using the Phonon module in the MedeA software package. This program applies the direct method [11] for calculating vibrational frequencies and uses forces calculated with VASP. Supercells extending approx. 10Å in each lattice direction were created to minimize the interactions between equivalent atoms in adjacent cells, and atoms are displaced 0.02Å from their equilibrium position for the force calculations.

Each Raman active mode for a particular complex is indicated by a vertical line in the figures with a height determined by the total phonon density of states (DOS). In this way a set of discrete lines which represent the Raman DOS is generated for comparison to all measurements. However, Raman matrix element effects have not been included and thus there may still be differences in the Raman intensity for a particular mode and the calculated DOS.

OXIDE RESULTS

In Fig. 1 is shown the Raman spectra of Nb₂O₅ and NbO₂ commercial powders along with the DFT calculations of the Raman DOS. The calculation assumes the P2 structure for Nb₂O₅. Overall there is excellent agreement between the Raman DOS and Nb₂O₅ powder, indicating the accuracy of the VASP calculations, however the intensities of the Nb-O bending modes between 600-700 cm^{-1} and the double bond stretch mode near 980 cm^{-1} are higher than the calculated Raman DOS probably due to matrix element effects. Lower frequency modes below 120 cm^{-1} are cut off in the Raman measurement. The presence of the 980 cm^{-1} mode in the NbO₂ powder indicates that oxidation of this powder has occurred after exposure to air. This is further confirmed by the weak double peak between 600-700 cm^{-1} , close to the two peaks of Nb₂O₅. Thus the NbO₂ Raman spectrum has a significant contribution of Nb₂O₅ modes and is best interpreted as a mixture of the two oxides.

The surface oxides of Nb were most clearly observed in Nb powders probably due to the larger surface oxide volume probed by Raman in such loosely packed arrangements. For example, the Nb metal is penetrated by

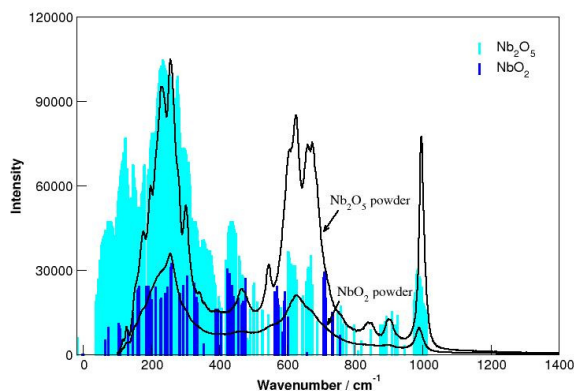


Figure 1: Experimental Raman spectra of Nb_2O_5 and NbO_2 powders (black lines) along with DFT calculations of the Raman DOS for Nb_2O_5 (light blue) and NbO_2 (dark blue).

The surface oxides of Nb were most clearly observed in Nb powders probably due to the larger surface oxide volume probed by Raman in such loosely packed arrangements. For example, the Nb metal is penetrated by the incident laser only up to a skin depth, whereas the insulating or semiconducting oxide layers are more transparent and thus would allow a much deeper penetration into the bulk, along the surface edges of each grain of the powder, giving a relatively larger Raman signal.

The Raman spectra of two Nb powders is shown in Fig. 2. In each case the Nb powder was exposed to an acid bath of the type used for EP etching followed by a water rinse. One of the Nb powders was subjected to a mild bake at 120 C in argon gas for 48 hr. What is most striking is that the etched Nb powder displays a Raman spectrum nearly identical to that of the NbO_2 powder data (rescaled) (black and red curves respectively). But it must be remembered that the NbO_2 powder had a significant Nb_2O_5 content. After baking, the Nb powder oxide spectrum shifts more toward the expected NbO_2 Raman DOS (blue lines). Note the loss of the 980 cm^{-1} mode after baking. We interpret this as a clear indication that the mild bake increases the NbO_2 thickness, consistent with x-ray scattering studies of Nb before and after a mild bake. [12]

HYDRIDE RESULTS

The ordinary Raman backscatter spectra from smooth regions of flat Nb pieces (single crystals, foils) is highly reproducible, but rather featureless. An example is shown in the bottom curve of Fig. 3. There is little evidence of the sharp phonon structures from the oxide layers as found in Nb powders, likely due to the reduced sample volume. A broad, higher frequency peak near 1350 cm^{-1}

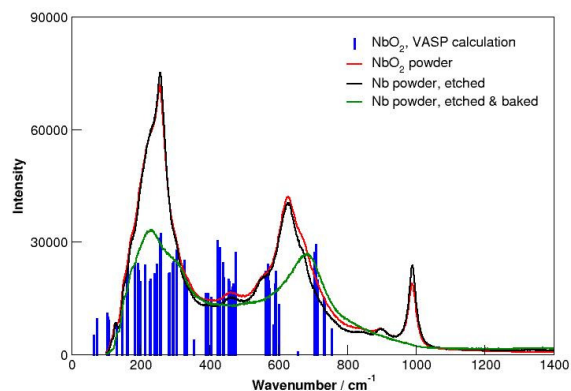


Figure 2: Raman spectra of Nb powder etched (black line) compared with NbO_2 powder rescaled (red line). Raman spectrum of baked Nb powder is shown as the green line while DFT Raman DOS is shown as blue lines.

is observed that is well beyond the oxide vibrational modes. However, a principal result of the present study is the reproducible observation of sharp Raman peaks between $1000\text{ -}1600\text{ cm}^{-1}$ in regions of such samples that we refer to as rough, an example of which is the top curve of Fig. 3.

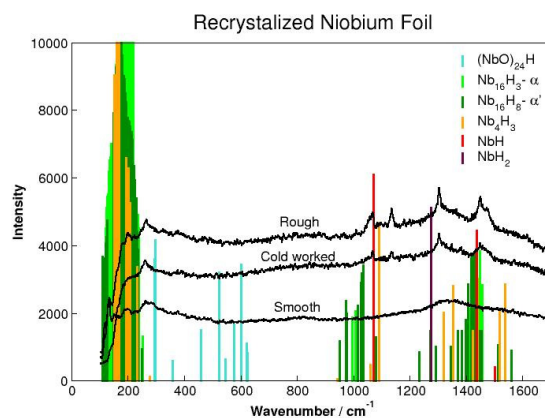


Figure 3: Raman spectra of EP recrystallized Nb foils. Bottom curve is from smooth region, middle curve is from cold worked region and top curve is from a rough spot (likely an etch pit). Raman peaks between $1000\text{ -}1550\text{ cm}^{-1}$ originate from Nb-H complexes as shown by the DFT Raman DOS (colored lines).

Such rough regions appear as dark spots under an optical microscope. Atomic force microscopy images of these spots reveal an RMS roughness 10-20 times greater than found in the smooth regions. Such rough spots are

likely to be etch pits in samples treated by BCP or EP, with the highest density of rough spots in BCP samples. Nearly identical Raman spectra are observed in regions of recrystallized Nb foils that have been subjected to cold working (e.g. bending of the foil back and forth 20 times). Calculations of the Raman DOS reveal that these modes are coming from Nb-H complexes as shown by the colored lines in Fig. 3. In particular, the peaks near 1050 cm^{-1} and 1450 cm^{-1} are consistent with the ordered compound NbH. Other peaks may originate from Nb₄H₃ and there may be contributions from the solid solution phases of dissolved H in bcc Nb (α and α'). The peak near 1120 cm^{-1} has not yet been identified but we note that there are a host of Nb-O-H complexes of varying concentrations that await DFT calculations.

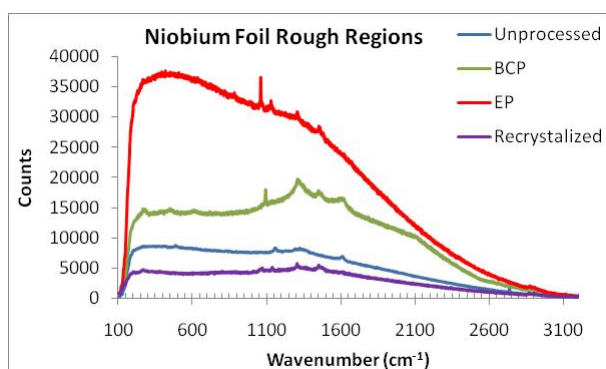


Figure 4: Raman backscatter spectra from rough spots of Nb foils subjected to various treatments. There is a consistent observation of sharp peaks in the range of $1000\text{--}1600\text{ cm}^{-1}$.

The hydride phases are consistently observed in rough spots of all Nb foils, including unprocessed, as indicated in Fig. 4. BCP treated foils have the highest density of rough spots and show relatively strong peaks in this region. The one common feature between rough spots (particularly etch pits) and cold worked regions of previously annealed foils is the likely presence of a high density of dislocations. The Raman data along with the DFT calculations lead to the conclusion that such regions attract hydrogen with sufficient concentration to form stable ordered hydride phases and the resulting inclusions in the bulk Nb are of sufficient size to be detected by ordinary Raman backscattering. This may explain the correlation between hot spots in SRF cavities and the presence of a high density of etch pits. Such inclusions are likely to lead to suppressed superconductivity, increased RF surface impedance, and thus local hot spot formation due to ohmic heating.

SURFACE ENHANCED RAMAN

The observations of section 3 indicate that hydride phases are observable in regions of high dislocation density. The question remains as to the extent of hydrogen in the subsurface of smooth regions of Nb foils or in single crystals, and the impact on the surface superconductivity. The ordinary Raman from such regions reveals a broad spectrum of relatively low intensity, likely consisting of amorphous oxides and hydrogen complexes. To elucidate these regions further we have successfully achieved surface enhanced Raman spectroscopy (SERS) using nanoscale Au islands. The use of deposited Au or Ag thin films ($\sim 10\text{ nm}$) to achieve SERS has been well documented in the literature. Such films produce islands of $\sim 10\text{ nm}$ diameter which resonate (plasma resonance) under the incident laser which leads to increased local electric fields and consequently enhanced Raman scattering from any molecular complexes either in physical contact with the metal island or near to it.

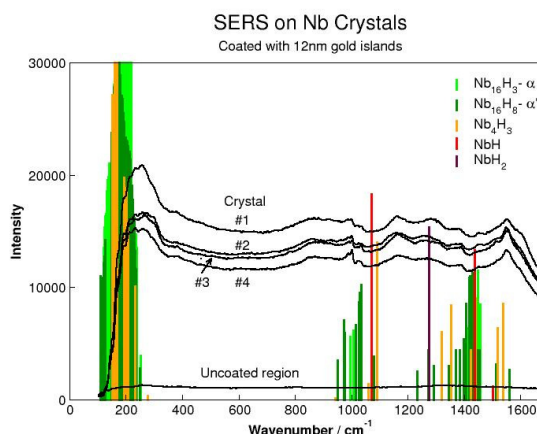


Figure 5: Surface enhanced Raman spectra (SERS) from Nb single crystals coated with $\sim 12\text{ nm}$ of Au. Note the enhancement of Raman intensity from typical uncoated spectrum. Crystals labeled #1 through #4 have been processed in different ways as discussed in the text.

In Fig. 5 is shown the Raman spectra from a set of Nb single crystals (labeled #1 through #4) that have been processed, exposed to laboratory air and subsequently coated with $\sim 12\text{ nm}$ Au film deposited at a rate of 0.3 \AA per second. The processing conditions are as follows: #1 (EP etch), #2 (EP+800 C vacuum anneal), #3 (EP+ mild bake), #4 (EP+800 C anneal+mild bake). The mild bake is at 120 C in Argon gas for 48 hr. The spectra display a significant enhancement of the Raman intensity by at least a factor of 5-10 compared with the ordinary spectrum, e.g. bottom curve of Fig. 5. In addition there is a highly reproducible set of peaks in the range of $1000\text{--}1600\text{ cm}^{-1}$ which, as discussed earlier, correspond to Nb-H complexes. However, in contrast to Figs. 3-4 on rough spots, the sharpest peaks appear to be from dissolved H phases (α and α') and peaks near ordered hydrides are

much broader. For example, the two peaks just below 1000 cm^{-1} can only be associated with α and α' phases and are relatively sharp.

Our present interpretation is that temporal behavior of the mobile H atoms must be considered. The underlying Nb is a stable bcc single crystal and the α and α' phases represent hydrogen occupying tetrahedral bonding sites. Such vibrational modes merely require the presence of hydrogen, on average, somewhere in the host Nb on a timescale longer than a few vibrational cycles and therefore would produce relatively sharp modes. On the other hand the vibrational modes from ordered hydrides would require a fluctuation into a different crystal structure completely and such a structure would be expected to have a much shorter lifetime and therefore broader peaks. In this picture the ordered hydride phases in smooth regions are not stable.

Remarkably, the SERS spectra appear to be independent of the processing conditions of the Nb single crystals. This is in contrast to the ordinary Raman which showed a strong dependence on processing, e.g., BCP foils exhibited a high density of rough spots with corresponding large peaks from ordered hydrides. This suggests that different processing steps (BCP, EP, baking) have the greatest impact on regions near grain boundaries where etch pits are likely to form.

SUMMARY AND CONCLUSION

Raman spectroscopy, in conjunction with DFT calculations of expected oxide and hydride phases, has been shown to be an effective probe of the Nb surface, relevant for SRF cavity development. A principal result of the present work is the observation of well defined Raman peaks originating from ordered hydride phases (e.g. NbH) in regions of processed foils that are likely to contain a high density of dislocations. Cold-worked regions, etch pits and other rough spots reveal the identical Raman spectra and strongly suggest that dislocations attract hydrogen and consequently a high dislocation density leads to high concentrations of hydrogen, sufficient to form stable, ordered Nb-H compounds. The present study offers an explanation for the correlation of hot spots in SRF cavities and the presence of a high density of etch pits. Such pits will likely have a subsurface consisting of a relatively higher concentration of hydride inclusions which will suppress the local superconductivity and increase the RF impedance leading to increased ohmic heating and hot spot formation.

We have also achieved a SERS signal on processed Nb crystals using a thin Au film. The SERS spectra on

smooth regions are identical, independent of the processing, and reveal dissolved hydrogen phases along with broadened peaks near Nb-H modes of hydride phases. This indicates that hydrogen is always present near the surface oxide layer but the concentration in the smooth regions is considerably smaller than found in pits. It also suggests that the impact of various processing steps (e.g. BCP vs. EP) mainly occurs at natural defects such as grain boundaries, where underlying dislocation densities are high and etch pits may form.

The Raman spectrum from Nb oxides was only clearly observed on Nb powders. This is attributed to the larger sample volume from the oxide layers in such loosely packed samples. A clear difference is found in the oxide spectrum after a mild baking procedure similar to that used in SRF cavities suggesting that the bake leads to a growth of the NbO₂ phase and a reduction of the Nb₂O₅ phase, consistent with other reports.

REFERENCES

- [1] Xin Zhao, G. Ciovati and T. R. Bieler, *Phys. Rev. STAB* **13**, 124701 (2010)
- [2] E. Ricker and G.R. Myneni, *J. Res. Natl. Inst. Stand. Technol.* **115**, 353-371 (2010)
- [3] R.J. Cava et al, *Phys. Rev. B* **44**, 6973 (1991)
- [4] T. Proslir, J.F. Zasadzinski, L. Cooley, C. Antoine, J. Moore, J. Norem, M. Pellin and K.E. Gray, *Appl. Phys. Lett.* **92**, 212505 (2008)
- [5] Kresse, G.; Furthmuller, J. *Phys Rev B* **54**, 11169 (1996).
- [6] Kresse, G.; Hafner, J. *Phys Rev B* **47**, 558 (1993)
- [7] Perdew, J. P.; Burke, K.; Ernzerhof, M. *Phys. Rev. Lett.* **1996**, *77*, 3865
- [8] Kresse, G.; Joubert, D. *Phys. Rev. B* **1999**, *59*.
- [9] Blöchl, P. E. *Phys. Rev. B* **1994**, *50*.
- [10] Monkhorst, H. J.; Pack, J. D. *Phys. Rev. B* **1976**, *13*, 5188
- [11] Parlinski, K.; Li, Z. Q.; Kawazoe, Y. *Phys. Rev. Lett.* **1997**, *78*
- [12] M. Delheusy, A. Steirle, N. Kasper, R. Kurta, A. Vlad, H. Dosh, C. Antoine, A. Resta, E. Lundgren and J. Andersen, *Appl. Phys. Lett.* **92** 101911 (2008)